Available online at www.sciencedirect.com

ScienceDirect

Ceramics International 40 (2014) 3485–3493

CERAMICS INTERNATIONAL

www.elsevier.com/locate/ceramint

Facile electrochemical synthesis of uniform β-$Co(OH)_2$ nanoplates for high performance supercapacitors

Mustafa Aghazadeh*, Somayeh Dalvand, Mojtaba Hosseinifard

Department of Chemistry, Faculty of Science, Islamic Azad University, Shahr-e-Ray Branch, Tehran, Iran

Received 9 August 2013; received in revised form 17 September 2013; accepted 18 September 2013
Available online 1 October 2013

Abstract

Uniform cobalt hydroxide nanoplates were prepared *via* pulse cathodic electrodeposition and their electrochemical performance was investigated using cyclic voltammetry and charge–discharge tests. The deposition experiments were performed in the pulse current (PC) mode by applying typical on-times and off-times ($t_{on}=5$ s and $t_{off}=10$ s). The mechanism of deposit formation and growth on the cathode surface is discussed in detail. The obtained deposit was characterized by CHN, XRD, IR, BET, SEM and TEM techniques. The analyses results revealed that the obtained deposit has a single phase of the hexagonal brucite-like β-$Co(OH)_2$ which is composed of completely uniform nanoplates with angles of adjacent edges of 120° and edge lengths ranging from 200 to 300 nm. The supercapacitive investigation by cyclic voltammetry and charge–discharge tests showed that the prepared nanoplates have high contribution of active materials in the redox reactions where they presented a high specific capacitance of 1012.7 F g^{-1} at current density of 2 A g^{-1} and an excellent cycling stability of 92% capacity retention after 1000 cycling. The average coulombic efficiencies of 99.5%, 94% and 90% were also observed for the 10th, 500th and 1000th charge–discharge cycles at the applied current density of 2 A g^{-1}. These findings verified the promising application of the prepared nanoplates as an electrode material for supercapacitors.

Keywords: E. Capacitors; Powders: electrochemical preparation; β-$Co(OH)_2$ platelets

1. Introduction

The properties of nanostructured materials are dependent on the shape of building blocks. Although many researches have been demonstrated, controlling the shape of building blocks is still a great challenge. In the past decade, one-dimensional nanostructures such as nanorods, nanowires and nanotubes have been intensively studied due to their novel properties and potential applications [1]. Two-dimensional nanoplates or nanosheets possess interesting properties because of their high anisotropy and ultra-thickness [2,3]. Nanoplates are considered as ideal systems for the investigation of dimensionally confined transport phenomena and as the ideal bases upon which to build functional devices. Therefore, it would be interesting to develop new methods for the synthesis of nanoplates of a variety of compounds.

$Co(OH)_2$ materials have been attractive in view of their layered structure with large interlayer spacing, their well-defined electrochemical redox activity, and the possibility of enhanced performance through different preparative methods [4–11]. An emerging application of $Co(OH)_2$ is an electrode material for electrochemical supercapacitors [12–15]. In the supercapacitive application, the sheet or plate-like structures are beneficial in improving the electrochemical performance of $Co(OH)_2$. These structures can provide large inter-sheet spacing for transferring the ions rapidly and increasing the electroactive material–electrolyte interface area i.e. electrolyte penetration which results in high utilization of the electrode materials. In addition to the inter-sheet spacing, the microstructure or morphology of the plates i.e. their thickness and porous nature has an important role in the electrochemical performance of these structures. It is obvious that thin and porous plates can result in a high surface area which produces large reaction sites and shortened ion diffusion paths, and a lot of pores cause better electrolyte penetration.

*Corresponding author. Tel./fax: +98 21 5522 9354.
E-mail address: mustafa.aghazadeh@gmail.com (M. Aghazadeh).

0272-8842/$ - see front matter © 2013 Elsevier Ltd and Techna Group S.r.l. All rights reserved.
http://dx.doi.org/10.1016/j.ceramint.2013.09.081

$Co(OH)_2$ is well-known to crystallize in two polymorphs, α and β [16,17]. The β form is a stoichiometric phase of the composition $Co(OH)_2$ with brucite-like structure and consists of a hexagonal packing of hydroxyl ions with Co(II) occupying alternate rows of octahedral sites [18,19], while the α-hydroxide is reported to be isostructural with hydrotalcite-like compounds that consist of positively charged $Co(OH)_{2-x}$ layers and charge balancing anions (e.g., NO_3^-, CO_3^{2-}, Cl^-, etc.) in the interlayer gallery [20–25]. The α-$Co(OH)_2$ is theoretically expected to exhibit superior electrochemical activity as compared to its β-counterpart because of its poorly or turbostratically crystallized structure. The α-$Co(OH)_2$ is metastable and easily undergoes a phase transformation into the more stable brucite-like β-$Co(OH)_2$ phase in strongly alkaline media. So, β-$Co(OH)_2$ is often selected as an additive of alkaline secondary batteries owing to its stability in alkaline electrolytes and enhanced conductivity when changed to β-CoOOH [26].

It has been identified that electrochemical behavior of $Co(OH)_2$ markedly depends on its grain size, morphology and crystal structure [27,28]. Since electric double-layer capacitance and pseudo-capacitance are both an interfacial phenomenon, the sheet or plate-like structures of $Co(OH)_2$ are beneficial in improving its electrochemical performance. In fact, these structures are inclined to form a layered structure that can provide large intersheet spacing for transferring the ions rapidly and increasing the electroactive material–electrolyte interface area. As a result, many attempts have been applied for the synthesis of layered nanostructures of $Co(OH)_2$. For example, several routes based on hydrothermal and solvothermal processes have been developed for the synthesis of nanosheets and/or nanoplates of $Co(OH)_2$ [29–32]. But there are only a few reports about the electrochemical synthesis (i.e. cathodic electrodeposition) of $Co(OH)_2$ nanoplates and investigation of their electrochemical behavior. Furthermore, to the best our knowledge, pulse cathodic deposition of $Co(OH)_2$ has been rarely studied. In fact, there is no research on the pulse cathodic deposition of $Co(OH)_2$. In the previous works, we applied galvanostatic cathodic deposition for the synthesis of layered nanostructures of $Co(OH)_2$ and found that porous nanosheets [33] and leaf-like nanostructures [34] of β-$Co(OH)_2$ are easily achievable by applying the current densities of only 2 and 1 mA cm^{-2}, respectively. The specific capacitances of 1047.3 F g^{-1} and 772.8 F g^{-1} were obtained for porous nanosheets and leaf-like nanostructures, respectively, in aqueous 1 M KOH within the potential range of −0.3 to 0.5 V (vs. Ag/AgCl) at the scan rate of 10 mV s^{-1}. Furthermore, we observed that cathodic deposition from low-temperature (10 °C) nitrate bath at the same condition applied in Ref. [34] results in uniform β-$Co(OH)_2$ disc-like nanoplates with nanostructures capable of delivering a specific capacitance of 736.5 F g^{-1} in aqueous 1 M KOH within the potential range of −0.2 to 0.5 V (vs. Ag/AgCl) at the scan rate of 10 mV s^{-1} [35]. In this work, we applied, for the first time, pulse current mode in the cathodic deposition of cobalt hydroxide from nitrate bath, and found that high surface area and uniform nanoporous nanoplates of β-$Co(OH)_2$ are easily achievable by this route. The supercapacitive performance of the prepared nanoplates was evaluated by cyclic voltammetry (CV) and charge–discharge techniques.

2. Experimental procedure

2.1. Chemicals

$Co(NO_3)_2 \cdot 6H_2O$ (Merck), polytetrafluoroethylene (PTFE, Merck), acetylene black and KOH (Merck) were used as received. All solutions were prepared by using purified water by a UHQ Elga System. Aqueous solution of 5 mM Co $(NO_3)_2 \cdot 6H_2O$ was prepared for electrodeposition.

2.2. Synthesis procedure

An electrochemical cell was constructed using a stainless-steel (316 L, size 1 cm × 1 cm × × 0.5 mm) cathode centered between two parallel graphite anodes. Prior to each deposition, the steel substrates were given a galvanostatically electropolishing treatment [33]. The deposition experiments were performed in the pulse current (PC) mode at typical on-times and off-times (t_{on} = 5 s and t_{off} = 10 s) with an average current density of 1 mA cm^{-2} (I_a = 1 mA cm^{-2}). After electrodeposition, the steel electrodes were brought out from the electrolyte and washed several times with deionized water, and dried at RT for 48 h. The deposit was then scraped from the steel electrode and subjected to further analyses.

2.3. Instrumentation

The crystal structure of the prepared samples was determined by powder X-ray diffraction (XRD, Phillips PW-1800) using Cu Kα radiation. The sample morphology was examined using scanning electron microscopy (LEO 1455VP) and transmission electron microscopy (TEM, Phillips EM 2085). Carbon, nitrogen, and hydrogen contents of the hydroxide powder were determined by CHN analysis (using Elementar Vario ELIII analyzer). FTIR spectrum was obtained by a Bruker Vector 22 FTIR spectrometer within the range of 400–4000 cm^{-1} wave numbers. The measurement of specific surface area for the prepared sample was performed through N_2 adsorption–desorption isotherms at 77 K with a Quantachrome NOVA-2200e system. Cyclic voltammetry (CV) and galvanostatic charge–discharge tests were performed by use of a potentiostat (AUTOLAB®, Eco Chemie, PGSTAT 30).

2.4. Electrochemical measurements

The electrochemical measurements were carried out in a three-electrode electrochemical cell containing 1 M KOH aqueous solution as an electrolyte. Ag/AgCl (1 M KCl, saturated) and platinum wire were used as the reference electrode and the counter electrode, respectively. The working electrode was prepared by mixing the prepared nanostructured $Co(OH)_2$, acetylene black, conducting graphite and polytetrafluoroethylene (PTFE) binder (with the weight ratios of

75:10:10:5, respectively). The total weight of the prepared mixture was 25 mg. The prepared mixture was pressed under 10 MPa into nickel foam current collectors (1 cm × 1 cm) and then dried in an oven for 10 min at 70 °C. The CV was conducted in a potential range between −0.2 and 0.6 V vs. Ag/AgCl at various scan rates of 2, 5, 10 and 25 mV s^{-1}. The constant current charge–discharge tests were carried out at different current densities of 1, 2, 5, 7 and 10 A g^{-1} within a potential range of −0.2 to 0.6 V.

3. Results and discussion

3.1. Hydroxide formation mechanism

The cathodic deposition of metal hydroxides involves two steps: electrochemical and chemical steps [36,37]. Measuring the potential values during the deposition process (Fig. 1a, −1.14 V vs. Ag/AgCl) revealed that the water reduction has a major role in the electrochemical step. The strings of gas bubbles on the cathode surface also confirmed this point. Fig. 1b shows the mechanism of cobalt hydroxide formation on the cathode surface. The electrochemical step includes water reduction and also production of OH^- ions and H_2 gas on the cathode surface (step **i** in Fig. 1b). This step results in an increase of local pH at the cathode surface. On establishing the pH conditions for $Co(OH)_2$ formation, the chemical step is started and cobalt hydroxide is sequentially formed and deposited on the cathode surface (step **ii** in Fig. 1b). The cathode potential value (−1.14 V vs. Ag/AgCl) disclosed that the nitrate ions have no role in the electrochemical step. However, they can contribute to the chemical step i.e. intercalation in the hydroxide structure (as schematically shown in Fig. 1b, step **ii**). To confirm the intercalation of nitrate ions, the obtained deposit was analyzed by CHN and the results showed 0.14% C, 2.81% H and 0.72% N in its composition. The existence of N in the deposit revealed that nitrate ions have intercalated in the chemical step as shown in Fig. 1b. It is worth noting that the pulse electrodeposition can provide better conditions for the hydroxide deposition [38,39]. In the PC deposition, the electrochemical step is periodically off (off-times, t_{off}) and no base is generated at these times of the electrodeposition process. These relaxation times of the electrochemical step cause the chemical step to occur in a controlled way. Also, during the off-times, Co^{2+} cations migrate to the depleted areas in the bath and more evenly distributed ions are available for deposition onto the cathode. So, it can be said that cobalt hydroxide has a sufficient time for the deposition and growth on the cathode surface in the chemical step of the electrodeposition process. In fact, the deposition and growth of cobalt hydroxide could occur with a special regularity, which give it a uniform and regular shape of morphology (as seen in the SEM images, Fig. 3). While, in the DC mode, the traffic exists for the deposition and growth of cobalt hydroxide on the cathode surface.

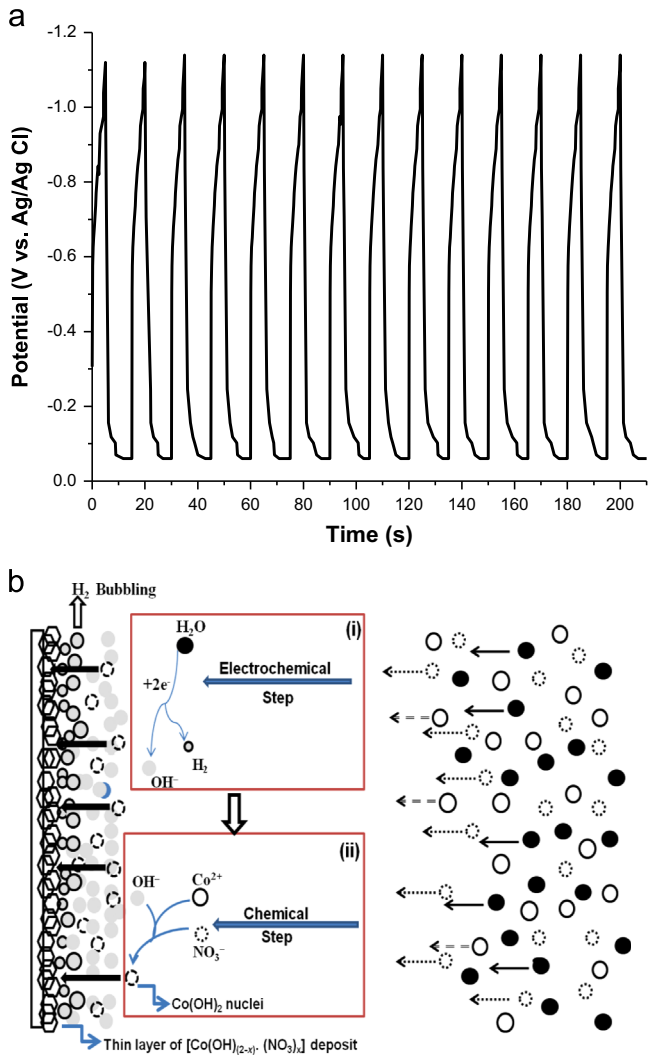

Fig. 1. (a) *V–t* profile during the pulse current electrodeposition of cobalt hydroxide and (b) schematic view of the deposition mechanism.

3.2. Characterizations

Fig. 2a shows XRD pattern of the hydroxide product. All the peaks can be indexed to pure brucite-like phase of β-$Co(OH)_2$ (hexagonal structure, JCPDS file no. 30-443). Compared with the standard pattern, intensity of the (0 0 1) peak is unusually stronger than others, implying the preferential orientation of (0 0 1) on the surface. No diffraction peaks of α phase are observed, indicating the high purity of the β phase that was successfully prepared at the applied pulse conditions. The FTIR spectrum of the prepared hydroxide is shown in Fig. 2b. The two peaks at 3439 and 1649 cm^{-1} are associated with the hydroxyl groups of molecular H_2O. The band at 659 cm^{-1} corresponds to the σ_{O-H} wagging vibration. The peaks at about 1480 and 1049 cm^{-1} are attributed to the carbonate groups originating from the reaction of oxide with air–CO_2 during the analysis procedure. The peaks at 1384 and 838 cm^{-1} are related to the ν_3 and ν_2 vibrational modes of NO_3^- intercalated in the interlayers [22]. A sharp peak observed at 3637 cm^{-1} is assigned to the hydroxyl group in the brucite-like structure. The peaks in the region of 480–540 cm^{-1} can be assigned to metal–oxygen vibrations and metal–OH bending vibrations in

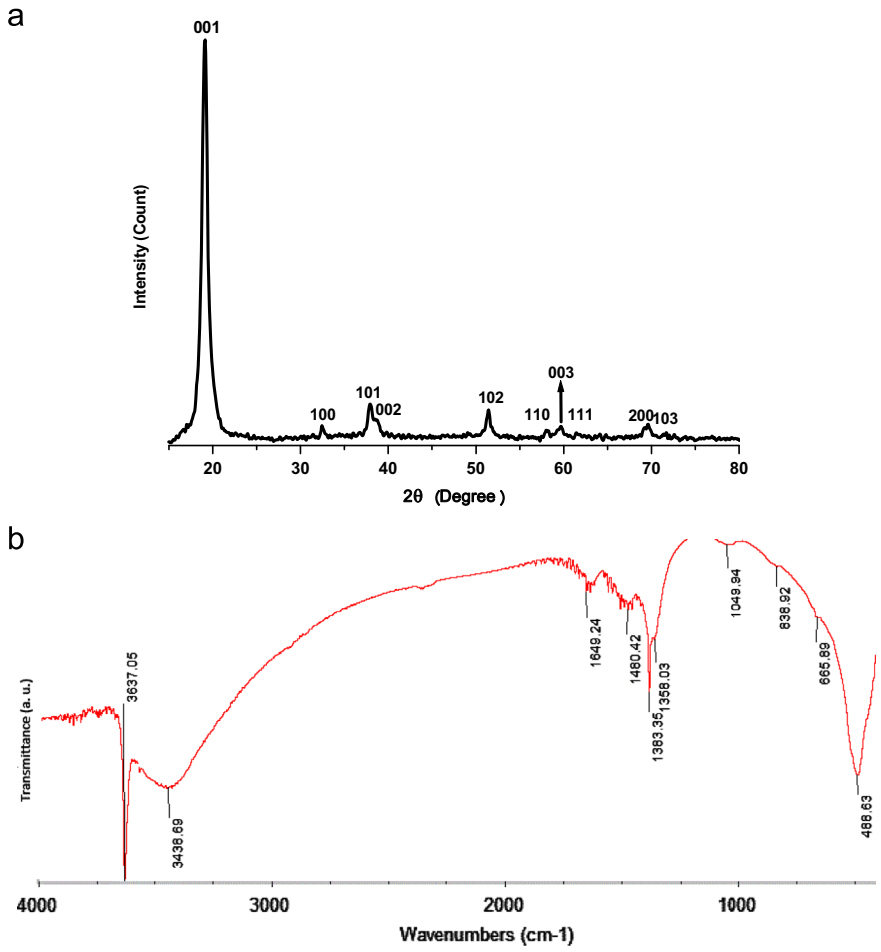

Fig. 2. (a) XRD pattern and (b) IR spectrum of the prepared hydroxide.

the brucite-like octahedron [41]. Thus, the FTIR measurement confirms the brucite-like structure of the product.

Fig. 3 shows the surface morphology of the prepared β-Co $(OH)_2$. The SEM images (Fig. 3a–c) show that the prepared hydroxide has layered morphology. In fact, a plate-like structure with regular uniformity is clearly seen in the SEM images. The plates are at nanoscale and formed the layered arrays. This configuration of β-$Co(OH)_2$ plates clearly disclosed that their deposition process occurred with a special regularity as a result of applying the pulse mode in the deposition experiments. As mentioned above, in the pulse deposition, the initially formed $Co(OH)_2$ in the electrochemical step has enough time for deposition and growth on the cathode during the off-times, whereas in the DC mode there is a traffic in the deposition of hydroxide. TEM observations (Fig. 3d) clearly show that the prepared $Co(OH)_2$ is composed of hexagonal plates at nanoscale. The plates are completely uniform and of well-defined hexagonal form with the sizes in the range of 200–300 nm. All the plates are regular hexagons with adjacent edges of angle of adjacent edges of 120° as indicated by arrows in Fig. 3d. From the SEM images (Fig. 3a–d), the thickness of the $Co(OH)_2$ plates was calculated to be 20–40 nm. For this purpose, the thickness of more than 50 plates was calculated.

The surface area of the oxide product was measured using the Brunauer–Emmett–Teller (BET) method. Representative N_2 desorption/adsorption isotherms and the corresponding BJH (Barret–Joyner–Halenda) pore size distribution curve of the $Co(OH)_2$ nanoplates are shown in Fig. 4. The N_2 isotherm of nanoplates has a type IIb form with a large H3 hysteresis loop, indicating the presence of nanoporous materials according to the IUPAC classification [40]. This form is normally associated with monolayer–multilayer adsorption on an open and stable external surface of a powder, which may be non-porous, macroporous or even microporous. Furthermore, type IIb isotherm is obtained with aggregates of plate-like particles, which possess non-rigid slit-shaped pores. Because of delayed capillary condensation, multilayer adsorption is able to proceed on the particle surface until a high p/p_0 is reached. When condensation occurs, the state of the adsorbate changes and desorption curve therefore follows a different path until the condensate becomes unstable at a critical p/p_0 (as seen in Fig. 4a). The H3 loop is usually given by the aggregates of platy particles or adsorbents containing slit-shaped pores [40]. Also, this loop does not terminate in a plateau at high p/p_0 and the limiting desorption boundary curve is therefore more difficult to establish as seen in Fig. 4a. The $Co(OH)_2$ nanoplates have a high BET surface area of 104 $m^2\,g^{-1}$.

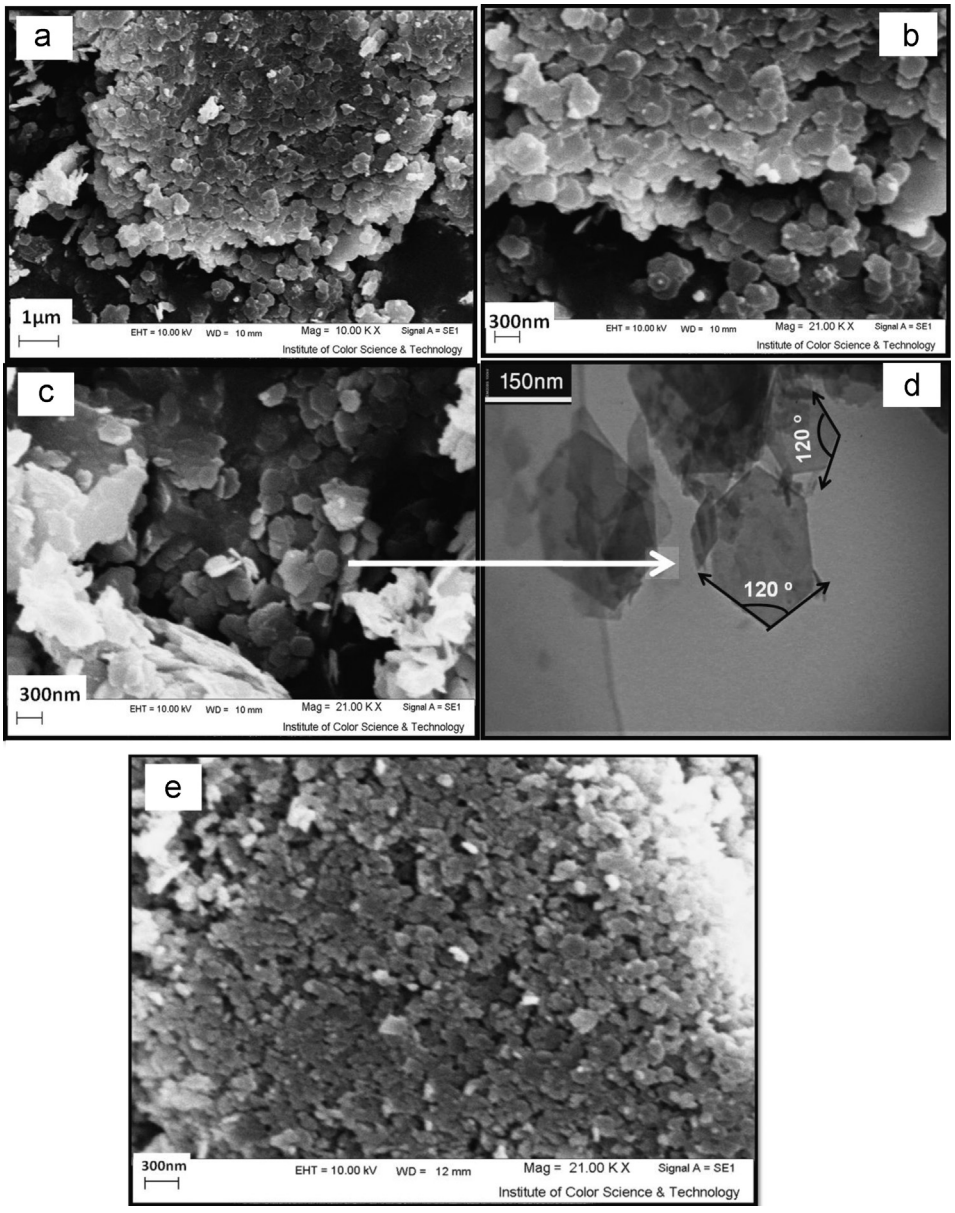

Fig. 3. (a)–(c) SEM and (d) TEM images of the prepared hydroxide, and (e) its SEM image after 1000 charge–discharge cycles.

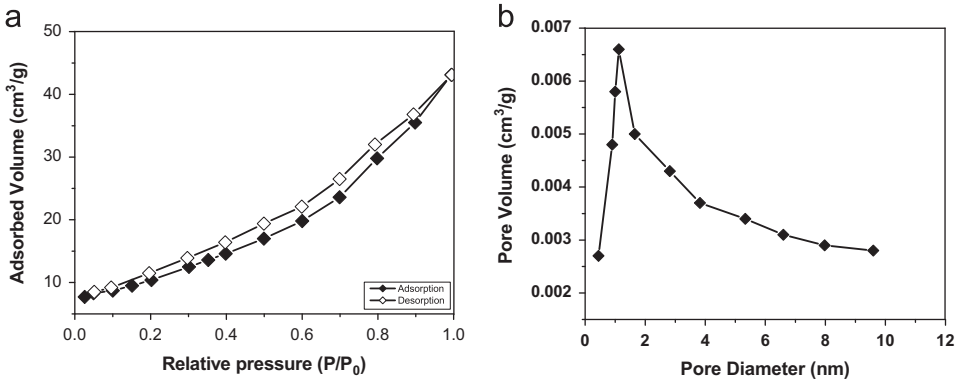

Fig. 4. (a) BET and (b) BJH pore size distribution curves of β-$Co(OH)_2$ nanoplates.

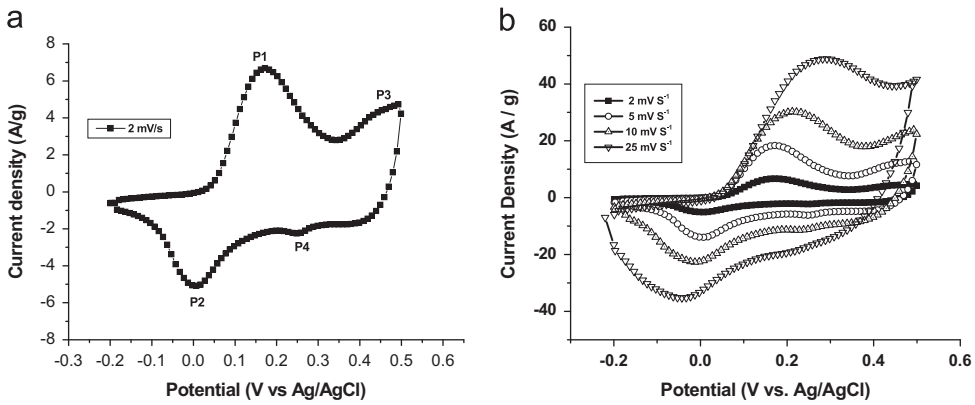

Fig. 5. (a) CV of β-$Co(OH)_2$ nanoplates at the scan rate of 5 mV s^{-1} and (b) at the various scan rates.

The pore size distribution, as calculated by the BJH method from the desorption branch of the nitrogen isotherm, revealed that the nanoplates contain pores with a size of 2.01 nm (Fig. 4b). These nano-pores may exist among small primary nanoparticles inside the $Co(OH)_2$ nanoplates. The nano-porosity and high specific surface area of the prepared nanoplates promise super-capacitive behavior.

3.3. Electrochemical evaluation

3.3.1. Cyclic voltammetry

Fig. 5a shows the CVs of the prepared β-$Co(OH)_2$ electrode in 1 M KOH at the scan rate of 2 mV s^{-1}. As seen in Fig. 5a, the β-$Co(OH)_2$ electrode exhibits two pair strong redox peaks due to the following Faradaic reactions of $Co(OH)_2$ [13–15]:

$$Co(OH)_2 + OH^- \underset{\text{discharge}}{\overset{\text{charge}}{\rightleftharpoons}} CoOOH + H_2O + e^- \quad (1)$$

$$CoOOH + OH^- \underset{\text{Discharge}}{\overset{\text{charge}}{\rightleftharpoons}} CoO_2 + H_2O + e^- \quad (2)$$

In Fig. 5a, the anodic peak P1 is due to the oxidation of β-$Co(OH)_2$ to β-CoOOH and the cathodic peak P2 is for the reverse process (Eq. (1)). The anodic peak P3 is due to the oxidation of β-CoOOH to CoO_2 and the cathodic peak P4 is for the reverse process (Eq. (2)). The CVs of the β-$Co(OH)_2$ nanoplates at various scan rates of 2, 5, 10 and 25 mV s^{-1} are also shown in Fig. 5b. The shape of the CV curves is not significantly influenced by increasing the scan rates, indicating that ionic conduction and electrolyte diffusion are improved a result of the high surface area and nanoporous structure of the prepared plates (as confirmed by BET and SEM). Also, a quasi-reversible electron transfer process is clearly observed in the CV curves, indicating that the measured capacitances are mainly based on the redox mechanism. The average specific capacitance of the prepared electrode was estimated from the CVs in Fig. 5b by integrating the area under the current–potential curve [12]:

$$C = \frac{1}{m\nu(V_a - V_c)} \int_{V_a}^{V_c} I(dV) \quad (3)$$

where C is specific capacitance of β-$Co(OH)_2$ (F g^{-1}) measured in the potential range of V_a–V_c, m is the mass of $Co(OH)_2$ (g), ν is the scan rate (V s^{-1}) and $I(V)$ is a current response depending on sweep voltage. Using Eq. (3), the specific capacitance of β-$Co(OH)_2$ nanoplates was calculated to be 1175.1, 1095.8, 1007.5 and 910.5 F g^{-1} at scan rates of 2, 5, 10 and 25 mV s^{-1}, respectively. These values demonstrated an excellent supercapacitive performance of the prepared nanoplates, which resulted from their nanoporous and high surface area (as confirmed by TEM and BET analyses). The electrochemical utilization of nanoplates was also calculated from the following equation [29]:

$$Z = \frac{C \times \Delta V \times M}{F} \quad (4)$$

where C is the real specific capacitance (F g^{-1}), ΔV is the potential window (0.7 V in this work), M is the average molecular weight of $Co(OH)_2$ (92.9 g mol^{-1}) and F is the Faradic constant (96,486 C mol^{-1}). Using Eq. (4), the electrochemical utilization of nanoplates was calculated to be 0.79, 0.74, 0.68 and 0.61 for the scan rates of 2, 5, 10 and 25 mV s^{-1}, respectively. These findings showed the excellent contribution of the electro-active sites in the redox reactions, thus giving the calculated high specific capacitances.

3.3.2. Charge–discharge tests

The galvanostatic discharge profiles of the β-$Co(OH)_2$ nanoplates were recorded at different current densities of 1, 2, 5, 7 and 10 A g^{-1} which are shown in Fig. 6a. All profiles present nonlinear curves, indicating that the capacitive behavior of the prepared $Co(OH)_2$ nanoplates is typically Faradaic pseudocapacitance. This behavior originates from the redox couples of Co^{4+}/Co^{3+} and Co^{3+}/Co^{2+}, which is completely in agreement with the CV curves (Fig. 5). Specific capacitances of the electrode at the applied current densities were

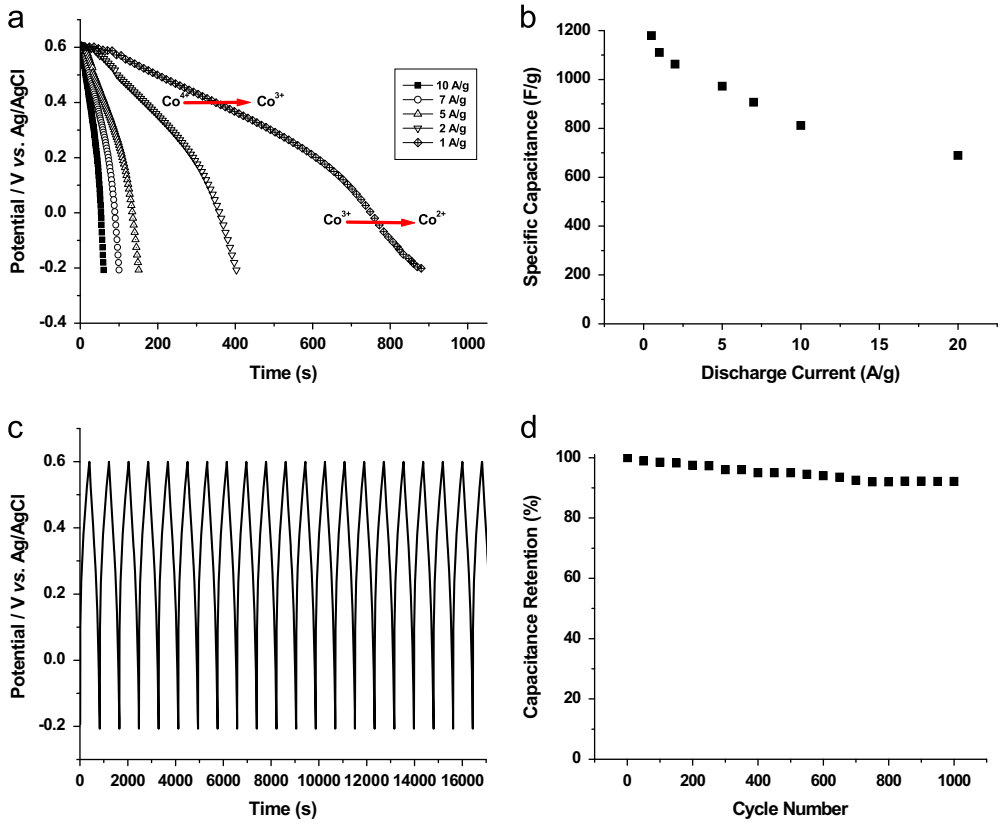

Fig. 6. (a) Discharge profiles of β-$Co(OH)_2$ nanoplates, (b) calculated capacitances at different current densities, (c) 1000 charge–discharge cycles at the current density of 2 A g^{-1} and (d) capacity retention during cycling.

calculated *via* the following equation:

$$C = \frac{I \times \Delta t}{m \times \Delta V} \quad (F/g) \tag{5}$$

where C is the specific capacitance, I is the applied constant current (A), ΔV is the potential range (0.8 V), Δt is the time of a discharge cycle (s) and m is the mass of β-$Co(OH)_2$ (g). The specific capacitance of the nanoplates was calculated using Eq. (5) and the results are shown in Fig. 6b. The results showed that the nanoplates are capable of delivering capacitances as high as 1105.3, 1012.7 and 979.1 F g^{-1} at the applied current densities of 1, 2 and 5 A g^{-1}, respectively (Fig. 6b). These values are in agreement with the calculated ones from the CVs (Fig. 5b) and also confirmed the excellent supercapacitive behavior for the β-$Co(OH)_2$ nanoplates. Furthermore, the observed capacitances are comparable with the reported ones for the nanostructured β-$Co(OH)_2$ prepared by different synthesis methods until now, for example, 591 F g^{-1} at 0.5 A g^{-1} for β-$Co(OH)_2$ nanoplates prepared by the sonochemical method [4], 690 F g^{-1} at 1 A g^{-1} for a β-$Co(OH)_2$ nanowall array prepared by pulsed laser deposition [7], 416.7 F g^{-1} at 5 A g^{-1} for β-$Co(OH)_2$ nanosheets prepared by sol–gel [10], 1084 F g^{-1} at 4 A g^{-1} for ordered mesoporous cobalt hydroxide (H_I-e $Co(OH)_2$) films prepared by potentiostatic cathodic deposition [14], 1164 F g^{-1} at 1 A g^{-1} for porous nanosheets of β-$Co(OH)_2$ prepared by galvanostatic cathodic deposition [33], 947.3 F g^{-1} at 1 A g^{-1} for leaf-like nanosheets of β-$Co(OH)_2$ prepared by galvanostatic cathodic deposition [34], 728.5 F g^{-1} at 1 A g^{-1} for disc-like nanostructures of β-$Co(OH)_2$ prepared by low-temperature cathodic electrodeposition [35], 726.1 F g^{-1} at 0.5 A g^{-1} for β-$Co(OH)_2$ nanoparticles prepared by the solvothermal method [41], and 1083 F g^{-1} at a current density of 0.83 A g^{-1} in 6 M KOH for β-$Co(OH)_2$ nanosheets electrodeposited on carbon nanotubes substrate [42].

As seen from Fig. 6b, the prepared nanoplates are capable of exhibiting specific capacitances of ~1180 F g^{-1} and ~680 F g^{-1} at the applied current densities of 0.5 and 20 A g^{-1}, respectively, indicating their high specific capacitive delivery and high-rate discharge capability. These excellent supercapacitive performances of the nanoplates are mainly originated from their high surface area and nanoporous surface which cause high electrolyte penetration, high contact of electrolyte/electrode and high electrochemical usage.

To investigate the long-term cycling stability of the β-$Co(OH)_2$ electrode, the galvanostatic charge–discharge cycling (1000 cycles) was recorded in 1 M KOH electrolyte at a constant current density of 2 A g^{-1} with the first 20 cycles presented in Fig. 6c. The specific capacitance of each cycle was calculated *via* Eq. (5) and, based on the obtained capacitances, the capacity retention of the β-$Co(OH)_2$ electrode on cycling was evaluated (Fig. 6d). The results showed that the prepared nanoplates have high stable capacitances during cycling where they exhibited excellent capacity retention of

ca. 92% after 1000 continuous charge–discharge cycles. Thus, it is concluded that β-$Co(OH)_2$ nanoplates can be suitable for long-time capacitor applications in KOH. Notably, morphological observations by SEM (Fig. 3e) revealed that no significant changes occurred in the morphology of β-$Co(OH)_2$ nanoplates after the charge–discharging process as compared with their initial morphology (see Fig. 3a–c).

The coulombic efficiency (η) was also calculated from the galvanostatic charge–discharge tests as follows [7,33]:

$$\eta = \frac{Q_d}{Q_c} \times 100 = \frac{\Delta t_d}{\Delta t_c} \times 100 \quad (6)$$

where Q_d and Q_c are the electric charge for discharging and charging, respectively. Δt_c and Δt_d are the times of charging and discharging, respectively. According to Eq. (6), the average coulombic efficiency was calculated to be about 99.5%, 94% and 90% for the 10th, 500th and 1000th charge–discharge cycles at the applied current density of 2 A g^{-1} (Fig. 6d).

The energy density (E) and power density (P) were calculated by the following equations from the constant current charge/discharge cycles [7,33]:

$$E = \frac{1}{2} C (\Delta V)^2 \quad (7)$$

$$P = \frac{E}{t} \quad (8)$$

Here, t and ΔV represent the discharge time and the potential range from the end of the charge to the end of the discharge, respectively. It can be found that the porous nanoplates can deliver energy and power densities of 0.972 Wh/g and 26.03 W/g, respectively. These results confirmed the excellent supercapacitive performance of the prepared nanoplates, which is related to their high surface area as well as porous and layered structure.

4. Conclusion

Uniform nanoplates of β-$Co(OH)_2$ were obtained by a two-step process: cathodic deposition followed by heat-treatment. The prepared nanoplates exhibited a specific capacitance of as high as 1012.7 F g^{-1} and good capacity retention of ca. 92% after 1000 continuous charge–discharge cycles at the applied current density of 2 A g^{-1}. These results confirmed the potential application of the prepared nanoplates as an electroactive material for supercapacitors.

References

[1] Y.N. Xia, P.D. Yang, Y.G. Sun, Y.Y. Wu, B. Mayers, B. Gates, Y.D. Yin, F. Kim, Y.Q. Yan, One-dimensional nanostructures: synthesis, characterization, and applications, Advanced Materials 15 (2003) 353–389.

[2] J.N. Coleman, M. Lotya, A. O'Neill, S.D. Bergin, P.J. King, U. Khan, K. Young, A. Gaucher, S. De, R.J. Smith, I.V. Shvets, S.K. Arora, G. Stanton, H.Y. Kim, K. Lee, G.T. Kim, G.S. Duesberg, T. Hallam, J.J. Boland, J.J. Wang, J.F. Donegan, J.C. Grunlan, G. Moriarty, A. Shmeliov, R.J. Nicholls, J.M. Perkins, E.M. Grieveson, K. Theuwissen, D.W. McComb, P.D. Nellist, V. Nicolosi, Two-dimensional nanosheets produced by liquid exfoliation of layered materials, Science 331 (2011) 568–571.

[3] M. Chhowalla, H.S. Shin, G. Eda, L.J. Li, K.P. Loh, H. Zhang, The chemistry of two-dimensional layered transition metal dichalcogenide nanosheets, Nature Chemistry 4 (2013) 263–275.

[4] C.C. Hu, J.C. Chen, K.H. Chang, Cathodic deposition of $Ni(OH)_2$ and $Co(OH)_2$ for asymmetric supercapacitors: importance of the electrochemical reversibility of redox couples, Journal of Power Sources 221 (2013) 128–133.

[5] W.J. Zhou, M.W. Xu, D.D. Zhao, C.L. Xu, H.L. Li, Electrodeposition and characterization of ordered mesoporous cobalt hydroxide films on different substrates for supercapacitors, Microporous and Mesoporous Materials 17 (2009) 55–60.

[6] Y. Wang, H. Wang, X. Wang, The cobalt oxide/hydroxide nanowall array film prepared by pulsed laser deposition for supercapacitors with superbrate capability, Electrochimica Acta 92 (2013) 298–303.

[7] C. Zhao, X. Wang, S. Wang, Y. Wang, Y. Zhao, W. Zheng, Synthesis of $Co(OH)_2$/graphene/Ni foam nano-electrodes with excellent pseudocapacitive behavior and high cycling stability for supercapacitors, International Journal of Hydrogen Energy 37 (2012) 11846–11852.

[8] L. Cao, F. Xu, Y.Y. Liang, H.L. Li, Preparation of the novel nanocomposite $Co(OH)_2$/ ultra-stable zeolite and its application as a supercapacitor with high energy density, Advanced Materials 16 (2004) 1853–1857.

[9] V. Gupta, S. Gupta, N. Miura, Al-substituted α-cobalt hydroxide synthesized by potentiostatic deposition method as an electrode material for redox-supercapacitors, Journal of Power Sources 177 (2008) 685–689.

[10] Z.A. Hu, L.P. Mo, X.J. Feng, J. Shi, Y.X. Wang, Y.L. Xie, Synthesis and electrochemical capacitance of sheet-like cobalt hydroxide, Materials Chemistry and Physics 114 (2009) 53–57.

[11] W.J. Zhou, J. Zhang, T. Xue, D.D. Zhao, H.L. Li, Electrodeposition of ordered mesoporous cobalt hydroxide film from lyotropic liquid crystal media for electrochemical capacitors, Journal of Materials Chemistry 18 (2008) 905–910.

[12] V. Gupta, T. Kusahara, H. Toyama, S. Gupta, N. Miura, Potentiostatically deposited nanostructured α-$Co(OH)_2$: a high performance electrode material for redox-capacitors, Electrochemistry Communications 9 (2007) 2315–2319.

[13] R.S. Jayashree, P.V. Kamath, Electrodeposition of ordered mesoporous cobalt hydroxide film from lyotropic liquid crystal media for electrochemical capacitors, Journal of Materials Chemistry 9 (1999) 961–963.

[14] W.J. Zhou, D.D. Zhao, M.W. Xu, C.L. Xu, H.L. Li, Effects of the electrodeposition potential and temperature on the electrochemical capacitance behavior of ordered mesoporous cobalt hydroxide films, Electrochimica Acta 53 (2008) 7210–7219.

[15] Z.A. Hu, Y.L. Xie, Y.X. Wang, H.Y. Wu, Y.Y. Yang, Z.Y. Zhang, Synthesis and electrochemical characterization of mesoporous $CoxNi_{1-x}$ layered double hydroxides as electrode materials for supercapacitors, Electrochimica Acta 54 (2009) 2737–2741.

[16] R. Ma, Z. Liu, K. Takada, K. Fukuda, Y. Ebina, Y. Bando, T. Sasaki, Tetrahedral Co(II) coordination in α-type cobalt hydroxide: Rietveld refinement and X-ray absorption spectroscopy, Inorganic Chemistry 45 (2006) 3964–3969.

[17] P. Oliva, J. Leonardi, J.F. Laurent, C. Delmas, J.J. Braconnier, M. Figlarz, F. Fievet, Review of the structure and the electrochemistry of nickel hydroxides and oxy-hydroxides, Journal of Power Sources 8 (1982) 229–255.

[18] P. Benson, G.W.D. Briggs, W.F.K. Wynne-Jones, The cobalt hydroxide electrode—I. Structure and phase transitions of the hydroxides, Electrochimica Acta 9 (1964) 275–280.

[19] C. Mockenhaupt, T. Zeiske, H.D. Lutz, Crystal structure of brucite-type cobalt hydroxide β-$Co\{O(H,D)\}_2$—neutron diffraction, IR and Raman spectroscopy, Journal of Molecular Structure 443 (1998) 191–196.

[20] J. Ismail, M.F. Ahmed, P.V. Kamath, Organic additive-mediated synthesis of novel cobalt(II) hydroxides, Journal of Solid State Chemistry 114 (1995) 550–555.

[21] M. Dixit, G.N. Subbanna, P.V. Kamath, Homogeneous precipitation from solution by urea hydrolysis: a novel chemical route to the α-hydroxides of nickel and cobalt, Journal of Materials Chemistry 6 (1996) 1429–1432.
[22] Z.P. Xu, H.C. Zeng, Interconversion of brucite-like and hydrotalcite-like phases in Co-hydroxide compounds, Chemistry of Materials 11 (1999) 67–74.
[23] Y. Zhu, H. Li, Y. Kottypin, A. Gedanken, Preparation of nanosized cobalt hydroxides and oxyhydroxide assisted by sonication, Journal of Materials Chemistry 12 (2002) 729–733.
[24] P. Jeevanandam, Y. Koltypin, Y. Mastai, Synthesis of α-cobalt(II) hydroxide using ultrasound radiation, Journal of Materials Chemistry 10 (2000) 511–514.
[25] R. Xu, H.C. Zeng, Dimensional control of cobalt-hydroxide-carbonate nanorods and their thermal conversion to one-dimensional arrays of Co_3O_4 nanoparticles, Journal of Physical Chemistry 107B (2003) 12643–12649.
[26] S. Hosono, I. Fujihara, M. Honma, H. Zhou, Synthesis of the CoOOH fine nanoflake film with the high rate capacitance property, Journal of Power Sources 158 (2006) 779–783.
[27] J.K. Chang, C.M. Wu, I.W. Sun, Nano-architectured $Co(OH)_2$ electrodes constructed using an easily-manipulated electrochemical protocol for high-performance energy storage applications, Journal of Materials Chemistry 20 (2010) 3729–3735.
[28] T. Zhao, H. Jiang, J. Ma, Surfactant-assisted electrochemical deposition of α-cobalt hydroxide for supercapacitors, Journal of Power Sources 196 (2011) 860–864.
[29] J. Wu, H. Zhang, N. Du, X. Ma, D. Yang, General solution route for nanoplates of hexagonal oxide or hydroxide, Journal of Physical Chemistry 110B (2006) 11196–11198.
[30] Z. Liu, R. Ma, M. Osada, K. Takada, T. Sasaki, Selective and controlled synthesis of α- and β-cobalt hydroxides in highly developed hexagonal platelets, Journal of the American Chemical Society 127 (2005) 13869–13874.
[31] B. Wang, H. Lin, Z. Yin, Hydrothermal synthesis of β-cobalt hydroxide with various morphologies in water/ethanol solutions, Materials Letters 65 (2011) 41–43.
[32] J.R.S. Brownson, C. Levy-Clement, Nanostructured α- and β-cobalt hydroxide thin film, Electrochimica Acta 54 (2009) 6637–6644.
[33] A.A. Malek Barmi, M. Aghazadeh, B. Arhami, H. Mohammad Shiri, A. Amini Fazl, E. Jangju, Porous cobalt hydroxide nanosheets with excellent supercapacitive behavior, Chemical Physics Letters 541 (2012) 65–69.
[34] M. Aghazadeh, A.A. Malek Barmi, T. Yousefi, Synthesis, characterization, and supercapacitive properties of β-$Co(OH)_2$ leaf-like nanostructures, Journal of Iranian Chemical Society 9 (2012) 225–229.
[35] M. Aghazadeh, H. Mohammad Shiri, A.A. Malek Barmi, Uniform β-$Co(OH)_2$ disc-like nanostructures prepared by low-temperature electrochemical route as an electrode material for supercapacitors, Applied Surface Science 273 (2013) 237–242.
[36] M. Aghazadeh, Electrochemical preparation and properties of nanostructured Co_3O_4 as supercapacitor material, Journal of Applied Electrochemistry 42 (2012) 89–94.
[37] H. Mohammad Shiri, M. Aghazadeh, Synthesis, characterization and electrochemical properties of capsule-like NiO nanoparticles, Journal of the Electrochemical Society 159 (2012) E132–E136.
[38] M. Aghazadeh, M. Hosseinifard, Electrochemical preparation of ZrO_2 nanopowder: impact of the pulse current on the crystal structure, composition and morphology, Ceramics International 39 (2013) 4427–4435.
[39] F. Khosrow-pour, M. Aghazadeh, B. Arhami, Facile synthesis of vertically aligned one-dimensional (1D) $La(OH)_3$ and La_2O_3 nanorods by pulse current deposition, Journal of the Electrochemical Society 160 (2013) D150–D155.
[40] F. Rouquerol, J. Rouquerol, K. Sing, Adsorption by Powders and Porous Solids, Academic Press, London, UK, 1999.
[41] S. Chen, J. Zhu, X. Wang, One-step synthesis of graphene−cobalt hydroxide nanocomposites and their electrochemical properties, Journal of Physical Chemistry 114C (2010) 11829–11834.
[42] J. Zhang, X. Wang, J. Ma, S. Liu, X. Yi, Preparation of cobalt hydroxide nanosheets on carbon nanotubes/carbon paper conductive substrate for supercapacitor application, Electrochimica Acta 104 (2013) 110–116.